Control of Nucleation in Solution Growth of Anatase TiO_2 on Glass Substrate

Hua Gui Yang and Hua Chun Zeng*

Department of Chemical and Environmental Engineering, Faculty of Engineering, National University of Singapore, 10 Kent Ridge Crescent, Singapore 119260, Singapore

Received: September 26, 2002; In Final Form: April 8, 2003

Low-temperature preparation of ceramic thin films in aqueous solution is an important new field in the synthesis of functional materials. This work examines control of nucleation in the growth of anatase titania (TiO_2) on a common glass substrate at 55−80 °C using an inorganic precursor, TiF_4. It is found that TiO_2 on fused silica is first formed as single-crystalline nuclei during an initial heterogeneous nucleation. These TiO_2 crystallites elongate along the [001] direction with their [110] axis perpendicular to the glass substrate; the elongated nuclei later grew into a round flowerlike morphology owing to a significant increase in homogeneous nucleation rate during the continued growth. The flowerlike polycrystalline TiO_2 islands, either as discrete crystallites or as lined crystallite arrays, subsequently develop into a planar crystallite monolayer. In general, low-pH condition suppresses heterogeneous nucleation and growth; this allows a self-alignment of thin threadlike crystallites. In contrast, higher pH favors the heterogeneous nucleation and subsequent planar growth but results in polydispersivity of crystallites. All of these observations can be related to the hydrolysis of TiF_4 and formation of Si−O−Ti and Ti−O−Ti linkages. In particular, localized HF concentration enrichment resulting from the TiF_4 hydrolysis is responsible for the sequential lined crystallite formation and planar-branching, as well as creation of unsaturated surface bonds of fused glass for heterogeneous nucleation. High nucleation densities have been achieved by mechanical and chemical treatments, and nanocrystalline TiO_2 thin films have been prepared using etched substrates.

Introduction

Formation of functional TiO_2 surface layers on ceramic or polymeric substrates or both has attracted much attention in recent years.[1−30] In particular, low-temperature synthesis and material-gradient fabrication are the two preferred approaches for the release of thermomechanical stress that developed at the interface.[1,7−30] There are two basic roles of a substrate in such syntheses: (i) material support and (ii) template, where the substrate either becomes an integrated part of final lamellar/film products or is removed in the process of fabricating shape-controlled functional materials. Depending on surface free energies of the overlayer, substrate, and their interface, the interaction between the overlayer and substrate is reflected in the initial nucleation processes and subsequent growth patterns. Ideally, this interaction should be controllable to meet different requirements of material preparations.[31]

Titanium dioxide (TiO_2) is an important functional material with a wide range of applications across vastly different fields such as thermal- or photocatalytic chemical reactions, gas sensors, pigments, dielectric ceramics, microelectronics, photonic materials, optical devices, solar energy conversion, hydrogen storage, inorganic membranes, environmental remediation, microorganism photolysis, and medical treatments because of its unique chemical, electronic, and optical properties.[1−30,32−43] In connection to these applications, there have been many techniques for fabrication of supported TiO_2.[1−30] For example, chemical vapor deposition (CVD), metal−organic chemical vapor deposition (MOCVD), molecular beam epitaxy (MBE), sputtering methods, spray pyrolysis, Langmuir−Blodgett transfer, adsorption−decomposition, sol−gel technique, and hydrothermal methods have been widely used in the preparation of TiO_2 thin films and shaped nanostructures.[1−21] In recent years, low-energy and environmentally friendly processes, such as liquid-phase deposition (LPD) analogous to "biomimetic" mineralization, have generated significant interests.[22−30] In particular, TiO_2 films and nanostructures with desired crystallographic phase(s) have been prepared by hydrolyzing titanium inorganic salts (e.g., $(NH_4)_2TiF_6$, TiF_4, and $TiCl_4$) in aqueous solution at low reaction temperature on various substrates that include metal oxides and organic polymeric materials.[22−30]

One of the fundamental issues during LPD processes is chemical interactions between Ti-containing species in aqueous phase and the surfaces of the original substrate or TiO_2-covered substrate or both. In the crystal growth process, these chemical reactions may be, respectively, related to the initial nucleation processes: heterogeneous nucleation and homogeneous nucleation. Although numerous studies have been devoted to the low-temperature LPD of TiO_2 using Ti inorganic salts,[22−30] most of these works focus only on the final TiO_2 products, and to the best of our knowledge, a detailed description of initial nucleation processes in this area is still lacking. Because the process information is extremely important in relation to the resultant crystallite size, shape, organization, and structural morphology, in this study, we examine the fundamental aspects of heterogeneous and homogeneous nucleations in LPD of TiO_2 on common glass substrates in relation to various preparative parameters.

Experimental Section

The formation reaction of TiO_2 was based on hydrolysis and condensation of titanium tetrafluoride (TiF_4).[44] Hydrochloric acid (HCl, 1.5 M) and aqueous ammonia ($NH_3 \cdot H_2O$, 1.5 M)

* To whom correspondence should be addressed. E-mail: chezhc@nus.edu.sg.

10.1021/jp022155u CCC: $25.00
Published on Web 10/15/2003

were used to adjust the pH of deionized water (1.0 L) to 2.1. TiF_4 (Aldrich Chemical) was then dissolved in this solution to give a concentration of 0.04 M, during which the pH was reduced to 1.8. Deionized water was used to adjust the concentration of TiF_4 to 0.002 63−0.0100 M before hydrolysis. Glass slides (about 22 mm × 22 mm in size, Menzel-glaser, Germany), which were washed with diluted alcohol, nitric acid, and deionized water, were immersed in the above TiF_4 solution (typically 40 mL) and maintained at 55−80 °C for a desired period of time. After the reaction, all of the samples were washed with deionized water and then air-dried at room temperature. To investigate the effect of surface defects, the glass slides were modified by a hydrothermal method. Typically, a clean glass slide was immersed in 30 mL of deionized water containing 0.1 g of thiourea (H_2NCSNH_2, Merck) in a Teflon-lined stainless steel autoclave. The autoclave was then kept at 200°C for a specified time (13−74 h). After hydrothermal modification, the glass slides were washed thoroughly with deionized water in an ultrasonic bath and then air-dried at room temperature. In addition to the above chemical method, a conventional glass knife (diamond cutter) was used to scratch the glass slide surface to create mechanically induced defects.

The crystalline phase of TiO_2 was determined by the X-ray diffraction method (Supporting Information).[45] The surface topography of the samples was examined with an atomic force microscope (AFM; DI NanoScope MultiMode) in the tapping mode to minimize damage of surface structures using the single-crystal silicon probe. On the average, AFM images from more than four sampling locations per sample were recorded to ensure a good representation of the surface topography.[46,47] Surface chemical analysis of TiO_2 on glass samples was performed by X-ray photoelectron spectroscopy (XPS; Supporting Information).[46] Morphological structures of the grown TiO_2 crystallites on glass substrate were also examined using a scanning electron microscope (SEM, JSM-5600LV, 15−20 kV) and a transmission electron microscope (TEM; JEM 2010, 200 kV).[48] The detachment of TiO_2 crystallites from glass substrate was carried out by sonicating TiO_2-deposited glass slides in acetone in an ultrasonic bath for 30 min. A drop of this TiO_2-containing suspension was placed onto a carbon 200-mesh copper grid and then dried at room temperature for TEM and electron diffraction (ED) investigation.[48]

Results and Discussion

From Linear to Planar Growth. Figure 1 shows a set of SEM images of TiO_2 crystallites grown on the glass slides at submonolayer to full-monolayer coverage (4−17 h reactions in 0.0100 M TiF_4 at 55 °C). With reaction time, the crystallites grow steadily in size and surface coverage. In the early growth, a large number of small TiO_2 crystallites with elongated morphology are found (4−5 h, Figure 1). The crystallites then grew into individual flowerlike islands "scattering" on the substrate "sea" and later merged together when the total population was increased, resulting in a monolayer structure (15−17 h, Figure 1).

One important observation from these SEM images is that the crystallites at any given time are always uniform. Considering this excellent monodispersivity, it is understood that the Ostwald ripening mechanism is operative throughout the growth. Smaller elongated crystallites tend to coalesce or dissolve or both during the growth, causing a crystallite population decline over the reaction time period of 4−7 h. The intercrystallite distance reaches a maximum of a few micrometers at 7 h (refer to Table 1). It can be concluded that no new heterogeneous nucleation on the glass surface occurs over this period (4−7 h). Considering the low deposition rate (in hours), the supersaturation of depositing species should be relatively low, and the growth can be considered to be in an equilibrium state. On the other hand, in the later stage of crystallite growth (8−17 h, Figure 1), polycrystalline instead of single-crystalline anatase crystallites with flowerlike structure appear (ED results, Figure 4), which implies that there is either an increase in supersaturation or an increase in energetically favorable nucleation sites with reaction time. The formation of the flowerlike crystallites can be attributed to homogeneous nucleation (new TiO_2 on existing TiO_2) taking place on some defect sites of the elongated crystallites formed earlier. Although TiF_4 has shown a relatively low hydration rate (strong bonding of Ti−F), it is still very difficult to maintain single crystallinity for individual TiO_2 crystallites with this precursor because of the lack of nucleation sites on the fused silica.

TABLE 1: Averaged AFM Spatial Data of TiO_2 Crystallites Grown in 0.0100 M TiF_4 Solution at 55 °C[a]

reaction time (h)	4	5	6	8	11	13
average base diameter (nm)	216/153[b]	306	398	653	740	996
average height (nm)	52	149	186	253	411	491
ratio of diameter to height	4.2/2.9	2.1	2.1	2.6	1.8	2.0

[a] Data are averaged spatial measurements from at least eight well-separated crystallites at each reaction time. Because of coalescence of TiO_2 crystallites at longer reaction times (e.g., 17 h, Figure 2), the diameter and height cannot be calculated accurately; the data for 15−17 h are not listed in this table. [b] Elongated crystallites (width = 153 nm; length = 216 nm).

Another important observation is that the TiO_2 crystallites grown on the glass substrate are not really "scattered"; in fact, they tend to arrange into somewhat self-assembled lines with minimum distance between them, as illustrated in Figure 1 (e.g., framed parts). This finding indicates that aside from the surface affinity between TiO_2 crystallites and the glass substrate through chemical bonds on the nucleation points, an interisland relation in a certain direction does exist. This observation will be further addressed later (Figures 4 and 5). When surface coverage increases (11−17 h, Figure 1), branching of these one-dimensional crystallite threads starts, forming larger two-dimensional islands that eventually develop into a crystallite monolayer. This process exhibits a layer-by-layer growth pattern or Frank−van der Merwe growth, in which the growth of a second TiO_2 layer (large white spots, 15−17 h, Figure 1) commences only after the completion of the first monolayer.

The crystallographic phase of the above TiO_2 crystallites is in anatase polymorph (XRD result; Supporting Information). Furthermore, XPS spectra of Ti 2p and Si 2p show that the amount of surface titanium increases gradually with the reaction time whereas the silicon content decreases accordingly. The peaks at BE = 458.5−458.8 eV can be assigned to Ti $2p_{3/2}$ of TiO_2,[2−4,30,39] while the ones at around BE = 103.0 eV can be assigned to Si $2p_{1/2}$ of the substrate SiO_2 (Supporting Information).[49] It should be mentioned that Si 2p photoelectrons can still be detected even after 17 h of reaction because the underlying glass substrate is not completely shielded by the TiO_2 overlayer.

AFM topographic images of TiO_2 crystallites grown on the glass substrate after different reaction times in 0.0100 M TiF_4 at 55 °C are shown in Figure 2, and their respective spatial data are tabulated in Table 1. In accordance with the SEM analysis (Figure 1), TiO_2 crystallites steadily increase in size

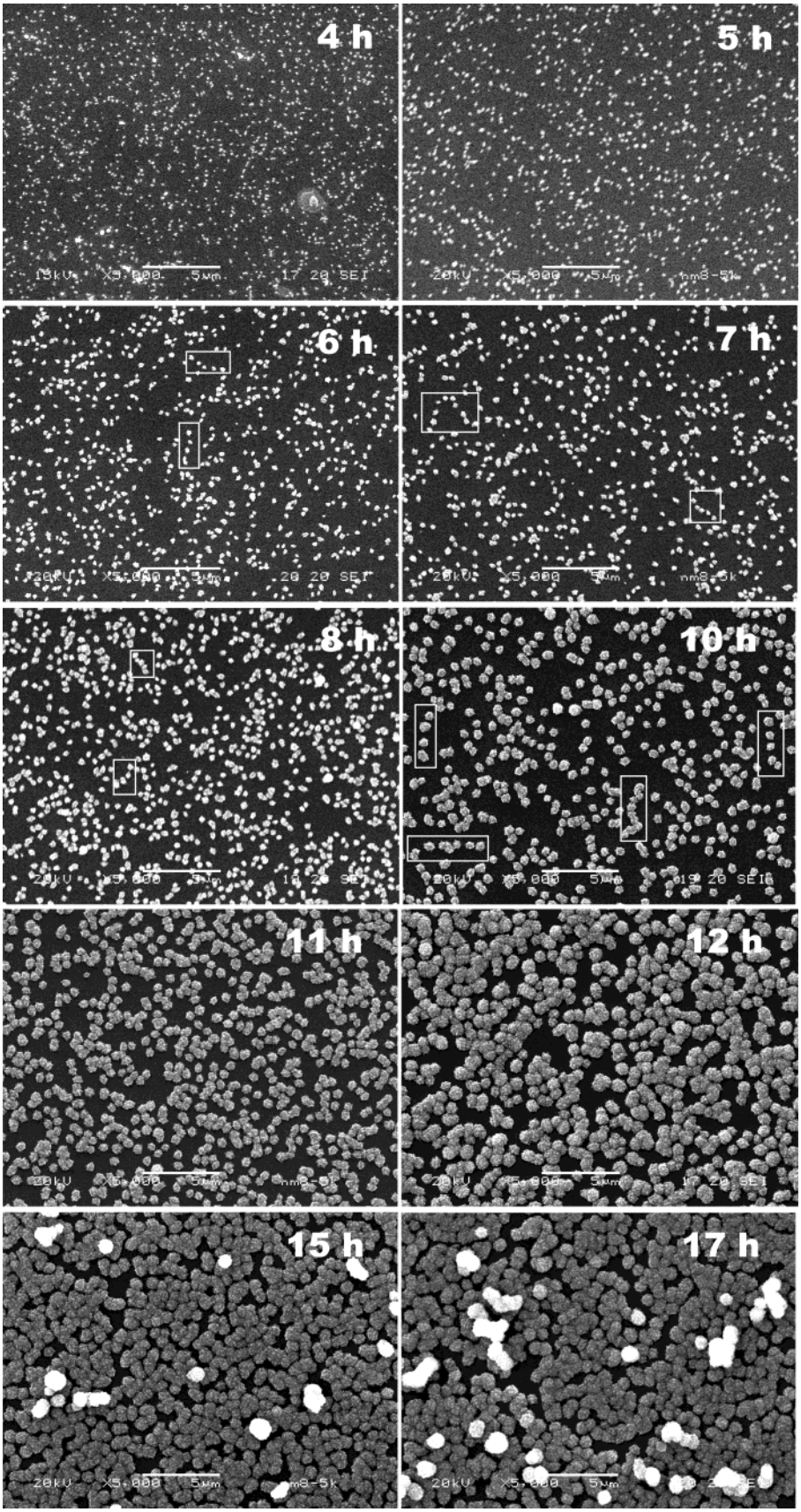

Figure 1. SEM micrographs of TiO_2 crystallites grown on glass slides after reactions in 0.0100 M TiF_4 at 55 °C for 4−17 h (pH = 2.0).

and eventually merge into each other forming the monolayer. Through AFM cross-sectional analysis, heights of crystallites (i.e., peaks) with respect to the substrate baseline can be measured accordingly (Table 1). Owing to an increase in crystallite size, the flat glass "valleys" between the "hills" disappear almost completely after 17 h.

One interesting finding from these spatial data (Table 1) is the abrupt change in the diameter-to-height ratio from 4.2 down

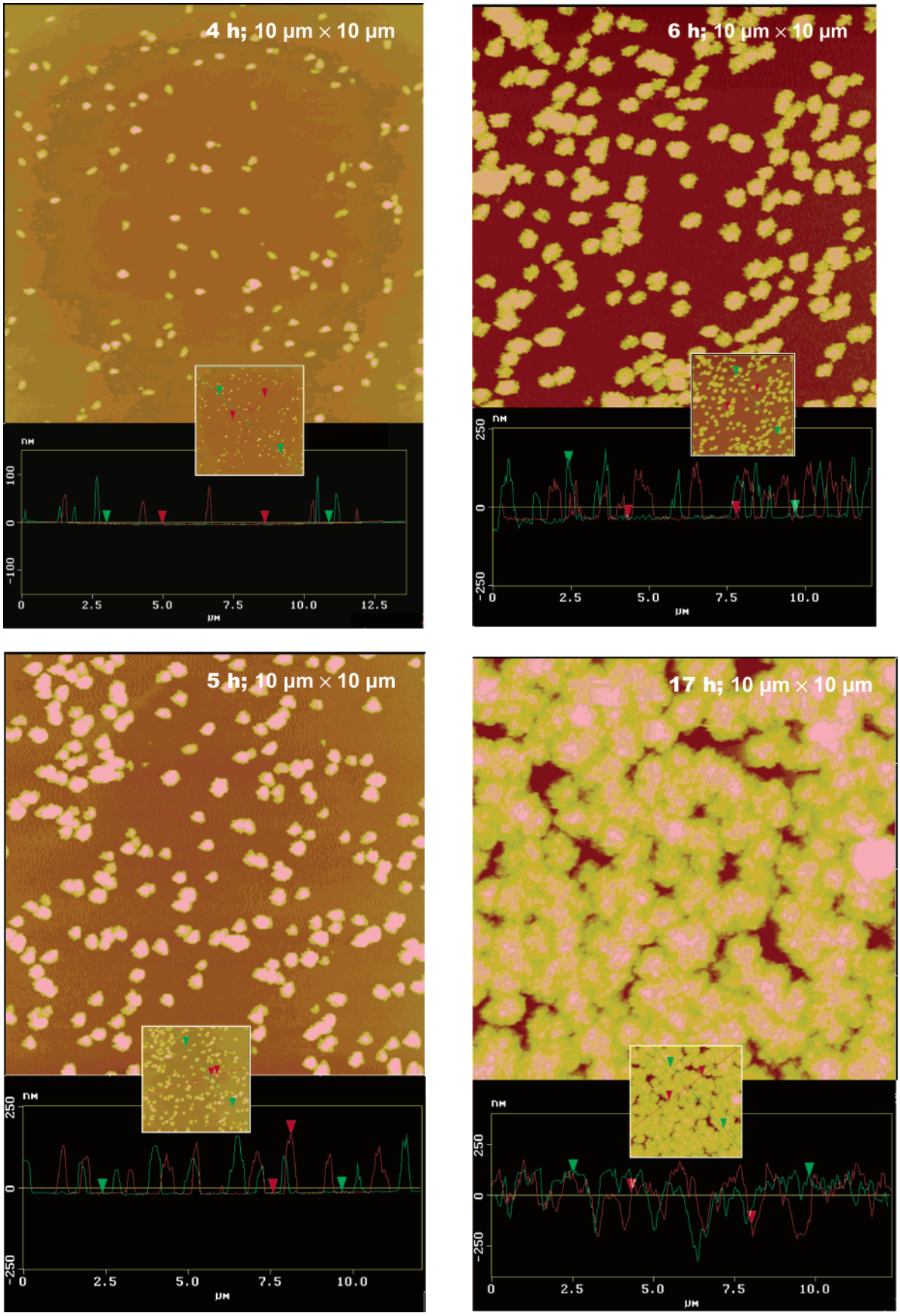

Figure 2. Representative AFM images and cross section profiles of TiO_2 crystallites on glass substrates after reactions in 0.0100 M TiF_4 (pH = 2.0) at 55 °C for 4−17 h.

to 2.1−2.6. In the beginning of growth (4 h), the large ratio of 4.2 reflects growth governed by the heterogeneous nucleation, because of the presence of pristine defect sites on the glass substrate. On the other hand, flowerlike crystallites are formed

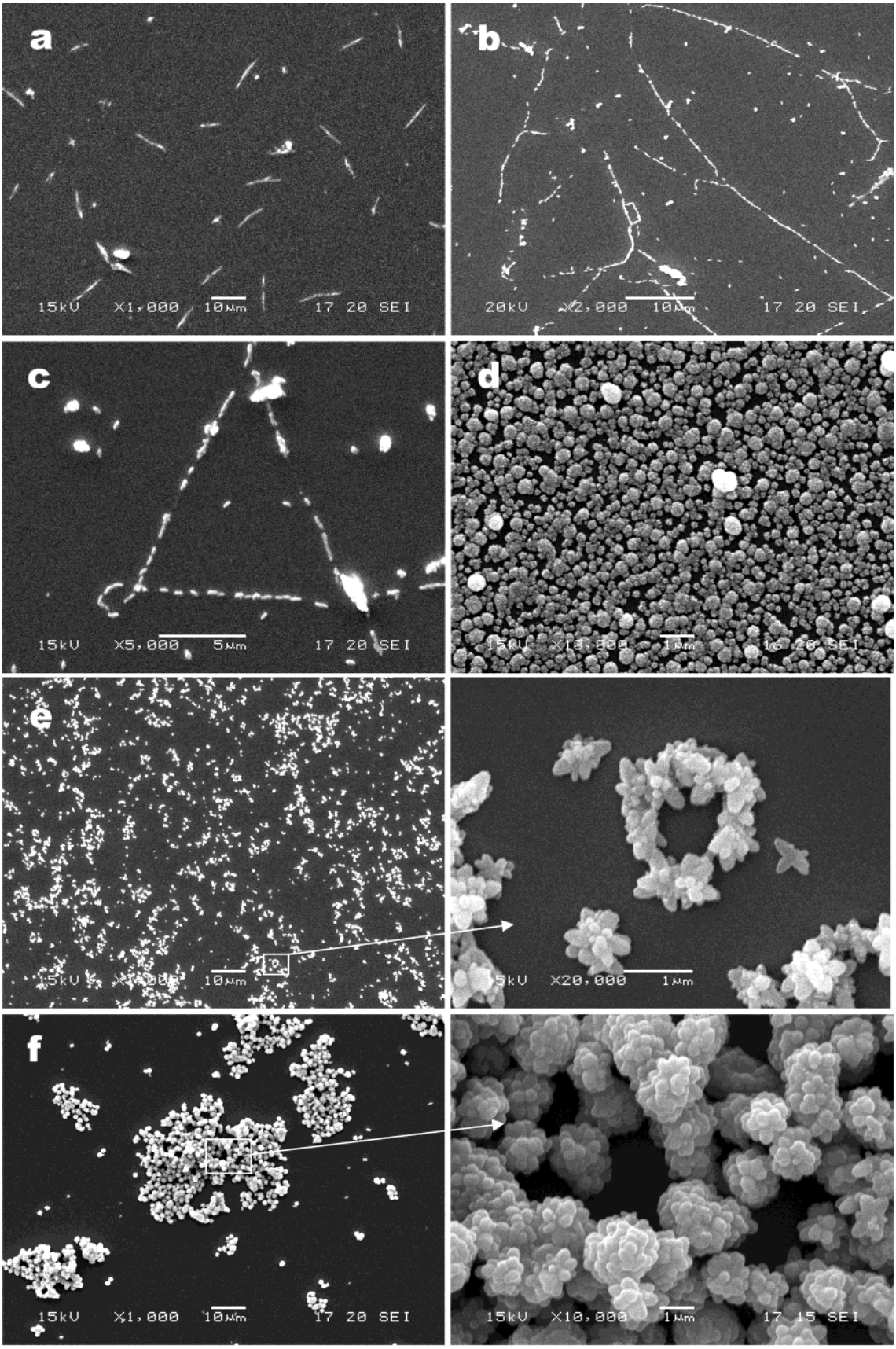

Figure 3. SEM micrographs of TiO_2 crystallites forming line patterns on glass substrates after 75 h reaction in 0.00526 M TiF_4 at 55 °C (a, pH = 1.3), 16 h reaction in 0.00263 M TiF_4 at 80 °C (b and c, pH = 1.3), 2 h reaction in 0.0100 M TiF_4 at 55 °C (d, pH = 2.5), 48 h reaction in 0.0100 M TiF_4 at 55 °C (e, pH = 1.5), and 24 h reaction in 0.006 M TiF_4 at 80 °C (f, pH = 1.5).

after this initial growth, which gives a smaller ratio of 2.1−2.6 owing to random homogeneous nucleation on the existing elongated crystallites (5−17 h). Thus, the abrupt change in this spatial ratio further indicates a change of growth mode in

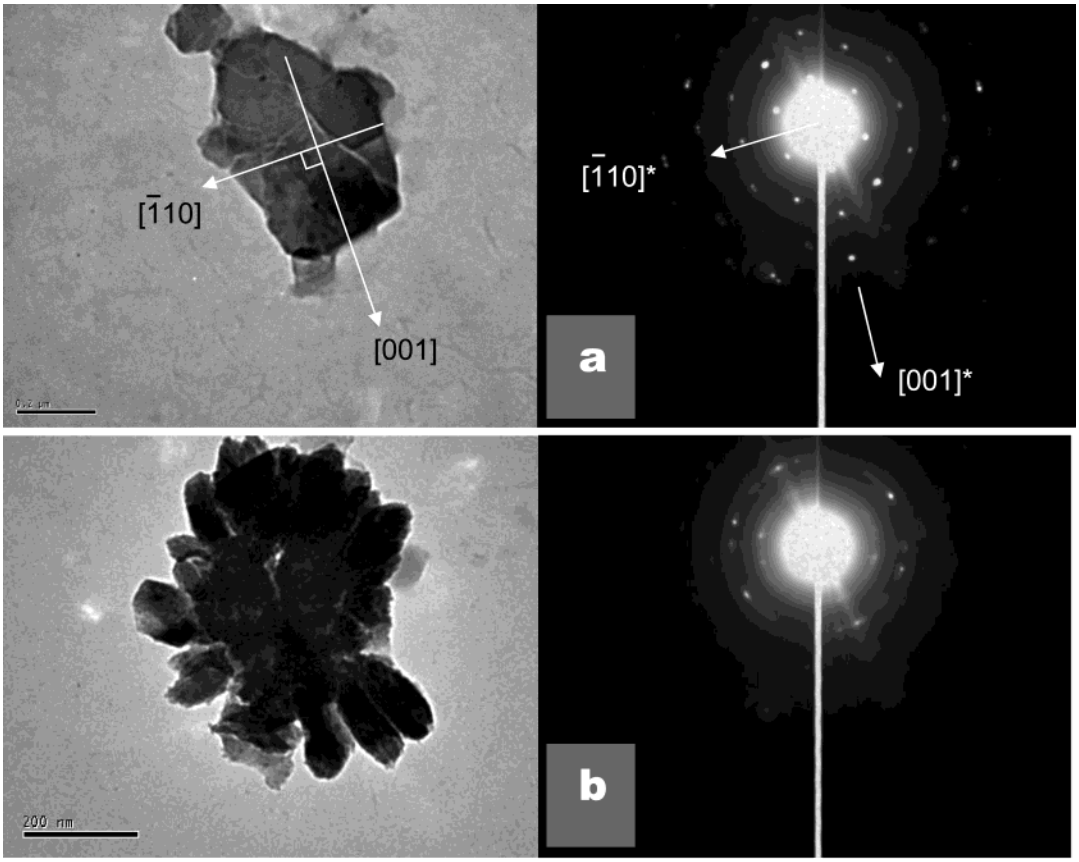

Figure 4. TEM images and corresponding ED patterns of TiO_2 crystallites formed after reactions in 0.0100 M TiF_4 (pH = 2.0) at 55 °C for 4 h (a) and 8 h (b).

excellent agreement with SEM/AFM morphological investigations.

Linear Assembly and Vertical Growth. Self-organizations of TiO_2 nanocrystals in liquid phase have been investigated recently with sol−gel and hydrothermal methods, which showed that surfactant-stabilized TiO_2 nanocrystallites can form various types of assemblies.[50] With the confinement of the silica substrate, we have observed a different type of TiO_2 crystal assembly in only one dimension (Figure 1), which will be further discussed below.

As mentioned earlier, the flowerlike TiO_2 islands are developed only after the formation of elongated crystallites. Presumably, the low degree of supersaturation should be the key to the initial formation of TiO_2 on the glass substrate where limited heterogeneous nucleation plays an active role. To further explore this phenomenon, a more dilute precursor solution was used in our next experiments with the anticipation that fewer primary crystallites will be formed. Indeed, reported in Figure 3a−c are TiO_2 crystallites up to a few tens of micrometers long (refer to Table 1) prepared under low-TiF_4 concentration and low-pH conditions. The elongated TiO_2 crystalline particles are arranged in a head-to-tail fashion (Figure 3c). Apart from this threadlike morphology, the growth mode observed here is essentially the same as the lined assemblies of flowerlike islands observed in Figure 1. It is interesting to note that these thread assemblies can even make unique turns on the glass substrates. Under these conditions, which do not seem favorable for the heterogeneous nucleation, the initial TiO_2 can only nucleate at the sites that are the most energy-favorable, resulting in only a few crystallites. Unlike those grown in 0.0100 M TiF_4 solution, these crystallites can be easily washed away from the glass substrate, indicating that there is only a weak contact between them. On the other hand, at higher pH (Figure 3d, pH = 2.5), rapid growth of TiO_2 is observed using a 0.0100 M TiF_4 solution. Comparing Figure 3d with Figure 1 (pH = 2.0), it is clearly demonstrated that the heterogeneous nucleation rate and thus the rate of TiO_2 deposition onto the glass substrate significantly increases with pH even though the TiF_4 concentration is kept constant. Nonetheless, this rapid heterogeneous nucleation results in serious polydispersivity of the TiO_2 crystallites within the same monolayer. In contrast to Figure 3d, heterogeneous nucleation can be suppressed when the pH is lowered. Figure 3e shows an example of the growth using the same 0.0100 M TiF_4 at pH = 1.5. As indicated in a crownlike TiO_2 crystallite assembly and a vertical growth, the heterogeneous nucleation is seriously inhibited, showing the Volmer−Weber-type growth mode. Even with a higher reaction temperature (Figure 3f), the heterogeneous nucleation is still not evidently promoted. In fact, the homogeneous nucleation seems to be more predominant, as indicated by the vertical growth and a significant increase in overall crystallite size.

Growth Mechanisms. The above investigations indicate two different morphologies of anatase TiO_2 crystallites under our synthetic conditions. As evident based on ED in Figure 4a, the first type of crystallites, which were grown in the beginning of the growth process (e.g., within 4 h, Figures 1 and 2) or under the low-pH conditions (e.g., Figure 3a−c), are single-crystalline TiO_2 elongated along the [001] direction. The diffraction pattern is indexed with two representative reciprocal axes, noting that reciprocal [001]* is parallel to the real space [001] of the examined crystallite.[11,12,51,52] Statistically, most of the detached TiO_2 crystallites give this type of diffraction pattern because they would use their flattened basis (i.e., the large surface formed in contact with the glass support) for free settlement during TEM

sample preparation (see Experimental Section). An identical pattern of this type has been observed for an anatase TiO_2 fiber bundle grown by a sol−gel template method, which indicates that the reciprocal crystal direction [110]* is always parallel to the incident electron beam.[11,12] In other words, the grown crystallite is lying on its (110) plane with [110] being perpendicular to the glass substrate. From the crystal axis assignment shown in Figure 4a, it is understood that the preferential growth direction is [001], which is in good agreement with commonly observed anatase mineralogical orientation [001]. The flowerlike crystallites, which were grown with prolonged reactions (5−17 h, Figures 1 and 2, Figure 3e−f) or under higher-pH conditions (Figure 3d), are indeed polycrystalline, as shown in Figure 4b. The polycrystalline nature is reflected in the diffraction rings resulting from the individual spots contributed by tiny crystallites that grew on the surface of single-crystalline seeds (Figure 4a).[23,51] As a result of random homogeneous nucleation on the external surfaces, apparently, these tiny crystallites are also elongated, presumably grown on some defect sites of the initial single-crystal nuclei (Figure 4a).

With the precursor compound TiF_4 used in this work, the following stepwise hydrolysis reactions are noted, similar to those for $(NH_4)_2TiF_6$:[44]

$$TiF_4 + H_2O \rightarrow TiF_3(OH) + HF \quad (1.1)$$

$$TiF_3(OH) + H_2O \rightarrow TiF_2(OH)_2 + HF \quad (1.2)$$

$$TiF_2(OH)_2 + H_2O \rightarrow TiF(OH)_3 + HF \quad (1.3)$$

$$TiF(OH)_3 + H_2O \rightarrow Ti(OH)_4 + HF \quad (1.4)$$

Ti^{4+} cations exist in aqueous solutions as six-coordinate complexes (e.g., $[Ti(OH_x)_6]^{(8-6x)-}$, a monomer) that can be further condensed into various polynuclear complexes such as corner-, edge-, and face-sharing octahedral dimers and trimers by olation or oxolation or both depending on the concentration of the solution.[53−56] Concerning the initial heterogeneous nucleation at the atomic level on the glass substrate, formation of Si−O−Ti linkages is the first essential step. Chemically, such heteroatomic bonding can result from a condensation between the two hydroxyl groups, ≡Si−OH and HO−Ti, or alternatively a nucleaphilic attachment of the oxygenated ligand $Si-O^-$ to a central Ti atom in the above precursor complexes or polynuclear complexes:

$$\equiv Si-OH + HO-Ti \rightarrow \equiv Si-O-Ti + H_2O \quad (2.1)$$

$$\equiv Si-O^-_{(substrate)} + TiF_{4-n}(OH)_n \rightarrow \equiv Si-O-Ti + F^- \quad (2.2)$$

On the other hand, the homogeneous nucleation and subsequent crystal growth depend on similar polycondensation and nucleaphilic attachment reactions, during which the homo-linkage of Ti−O−Ti is formed:

$$Ti-OH + HO-Ti \rightarrow Ti-O-Ti + H_2O \quad (3.1)$$

$$Ti-O^-_{(crystal)} + TiF_{4-n}(OH)_n \rightarrow Ti-O-Ti + F^- \quad (3.2)$$

For single crystals of network silica (such as cristobalite polymorph), it is expected that a significant amount of surface O or Si atoms or both are highly undercoordinated owing to the loss of atoms on truncated surfaces. Such unsaturated atoms, in principle, can act as atomistic heterogeneous nucleation centers for the growth of TiO_2 because of their strong bonding capabilities. For the fused glass fabricated by the hot-pressing process, however, the majority of O and Si atoms on the hot-pressed surface region are still chemically saturated owing to the fluidity of supercooled liquid upon roll-quenching,[57] and the pristine surface defects are limited in number. This is elucidated clearly in the density of nucleation sites revealed in our SEM/AFM investigations (4 h, Figures 1 and 2). The isoelectric point of silica is pH = 2,[58] which is the value used in most experiments of the present work. At pH ≤ 2, hydroxyl groups become abundant on the silica surface (Si−OH),[58] which apparently promotes the polycondensation reaction for the heterogeneous nucleation (eq 2.1). On the other hand, at pH > 2, the silica surface becomes negatively charged ($Si-O^-$)[58] and the nucleaphilic attachment becomes operative (eq 2.2) for the formation of Si−O−Ti bonding.

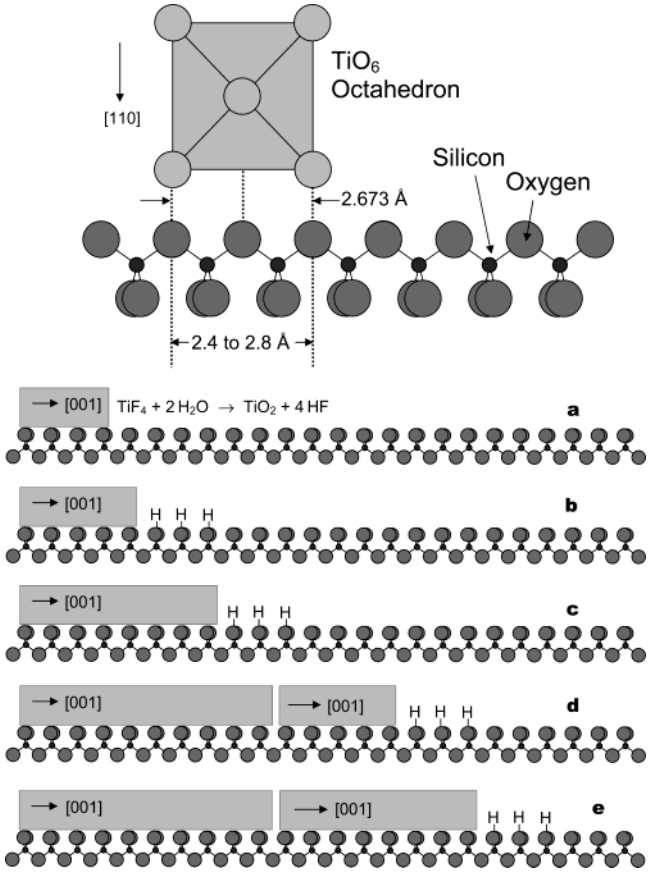

Figure 5. Structural model (top) of the common oxygen distances between [110]-oriented TiO_2 and silica substrate; the TiO_6 octahedron is viewed along [001] direction of anatase TiO_2. The bottom panel shows a proposed growth mechanism of lined assemblies of TiO_2 crystallites along [001] owing to a localized $[H^+]$ enrichment along the rapid growth direction [001].

On examination of bond lengths and bond angles of O−Si−O in polyhedral structures of transition metal (IV) silicates, we notice that the distance between two bridging oxygen atoms on the silica surface is about 1.2−1.4 Å.[59,60] Twice this distance matches the nearest distance between two oxygen atoms in a TiO_6 octahedron with the [110] direction perpendicular to the glass substrate, as illustrated in Figure 5. Because hydrolysis of TiF_4 produces HF, a localized enrichment in proton concentration $[H^+]$ in front of a growing interface is expected. Because the [001] axis is the preferential growth direction for the anatase crystallites, more protonated bridging oxygen atoms on the silica surface near the crystallite growth front are converted to silinol groups (Si−OH),[58,61] which will then serve as heterogeneous nucleation sites for sustainable growth, as depicted in Figure 5.

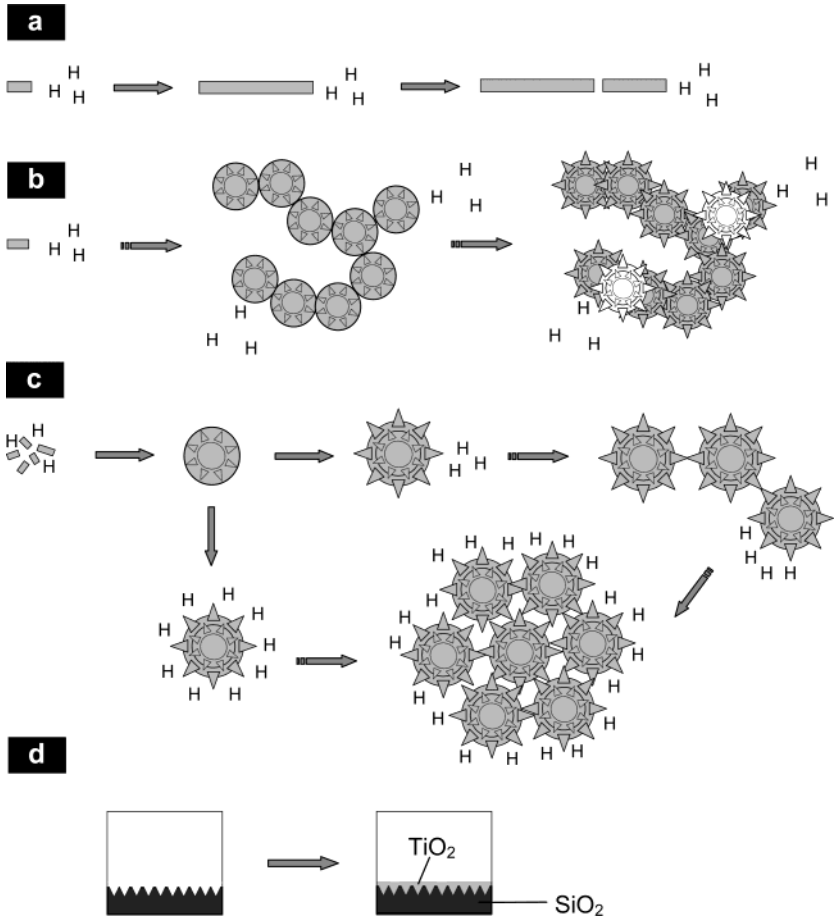

Figure 6. Schematic illustrations of growth modes of TiO_2 crystallites on glass substrate: (a) linear assemblies formed under low-pH conditions; (b) polycrystalline island extension under low-pH conditions and high reaction temperature; (c) polycrystalline island formation at isoelectric point; (d) creation of atomistic defects for simultaneous nucleation and the growth of a flat film.

Owing to the presence of surface defects, the Si−OH nuclei formed do not necessarily continue on the same track, resulting in a continuous but not always straight-line assembly.

Under low-pH conditions (e.g., pH = 1.3−1.5, Figure 3a−c), hydrolysis of TiF_4 becomes difficult, that is, equilibriums of eqs 1.1−1.4 will shift to the left because of the common ion effect. This type of growth corresponds to a low nucleation density case under low supersaturation conditions. On close examination of these "head-to-tail" assemblies, it is deduced that the nucleation sites are in fact created sequentially during the growth process, as depicted in Figure 6a, not the preexisting lined defect sites. If the latter was the case, the crystallites would have been grown with random orientations (also next subsection). Under the same low-pH condition but with a higher reaction temperature, both heterogeneous and homogeneous nucleations can be observed, but it is still very difficult to grow crystallite islands in a planar manner. This is evident in Figure 3e,f and illustrated in Figure 6b; note that the vertical growth (stacking) of a crystalline particle on an existing chain still belongs to the linear extension (Figure 6b).

At higher pHs (e.g., pH = 2.0−2.5, Figures 1, 2, and 3d), the degree of supersaturation is increased because the hydrolysis of TiF_4 becomes easier. This is reflected in the significant increase in nucleation density in these experiments. As illustrated in Figure 6c, the continuous growth of existing single-crystalline nuclei will lead to the formation of polycrystalline flowerlike crystallites owing to the coalescence of these randomly oriented seeds and defect sites on the crystallite surfaces. On the other hand, the localized $[H^+]$ variation on the glass surface still plays an important role in the formation of the line assemblies observed in Figure 1 (framed areas, 6−10 h). The gradual increase in nucleation density is evident in the planar growths at 11−17 h in Figure 1, when more TiF_4 molecules are hydrolyzed. As illustrated in Figure 6c, in particular, there are two modes of planar aggregation. The flowerlike crystallite chains are making turns as the remaining surface becomes scarce, which leads to the formation of planar assemblies. Similarly, a discrete crystallite or an existing crystallite assembly branches off in some or all directions, giving rise to the second growth mode.

In addition to its acidity, another effect of the resultant HF on the TiO_2 growth is its special ability to chemically etch the silica surface. This could be the reason that few published studies used TiF_4 as the precursor to make titania instead of alkoxides or chlorides. The localized HF concentration enrichment will also cause atomistic defects that can serve as heterogeneous nucleation sites for Si−O−Ti interconnection, including the formation of Si−F bonds. Nonetheless, this additional chemical etching must strike a balance between the formation of Si−O−Ti on the surface and depletion of Si−O−Si (and thus removal of formed Si−O−Ti) from the surface. It has been observed that under low-pH conditions (pH = 1.3, 45−75 °C, 0.002 63−0.005 26 M TiF_4, and 16−75 h), significant in-depth etching of a glass substrate also takes place. In certain cases, complete elimination of TiO_2 crystallites is found, as evident in the fish-bone-like deep etched pits of Figure 7a. Therefore, a localized proton enrichment can also be viewed as the creation of localized atomistic defects for the growth (Figures 5 and 6).

To generate a nanocrystalline TiO_2 monolayer, one must be able to promote simultaneous heterogeneous nucleation in two

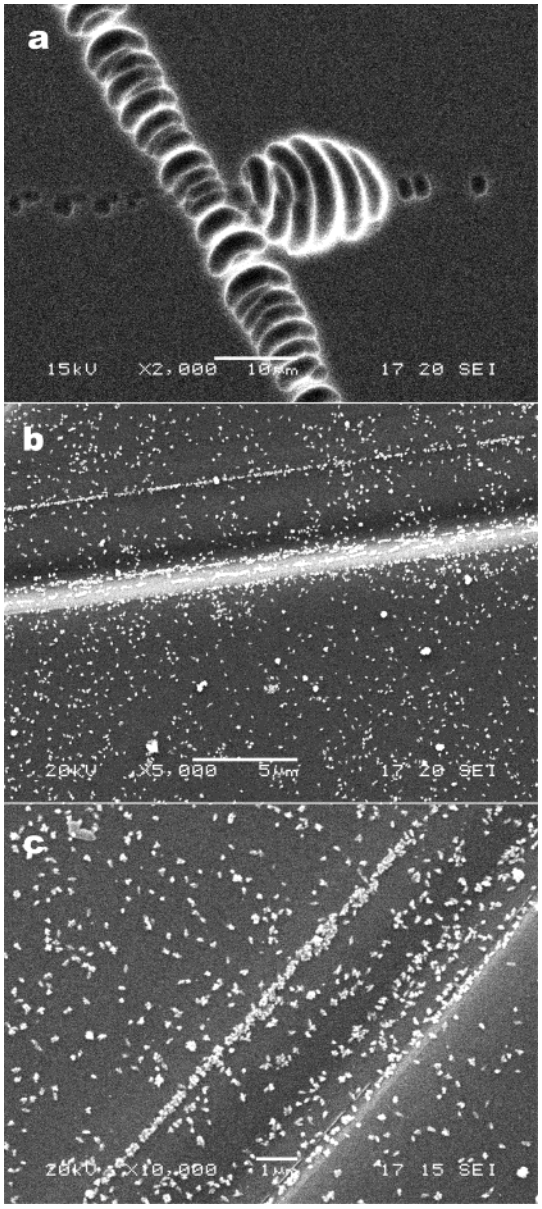

Figure 7. SEM images of a HF etched glass slide surface after 75 h reaction in 0.00526 M TiF_4 at 55 °C (a, pH = 1.3) and TiO_2 crystallites formed on the scratched glass slides after 4 h reaction in 0.0100 M TiF_4 at 55 °C (b and c, pH = 2.0).

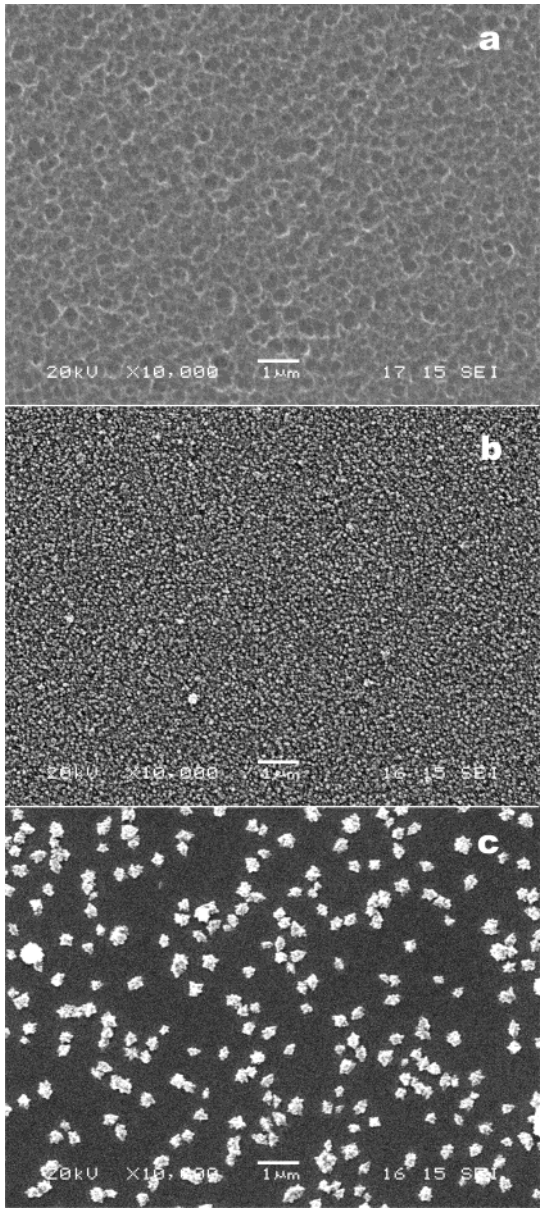

Figure 8. SEM images of glass modified by thiourea under 200 °C for 13 h (a), sample a after 3 h reaction in 0.0100 M TiF_4 at 60 °C (b, pH = 2.0), and unmodified glass slides after 3 h reaction in 0.0100 M TiF_4 at 60 °C (c, pH = 2.0).

dimensions. On the basis of the above findings, it seems that the growth at the isoelectric point (pH = 2.0) is highly favorable for synthesis of anatase crystallites with monodispersivity, but the sequential nucleation is still a major obstacle for the formation of nanosized crystallites. Ideally, as proposed in Figure 6d, a significant increase in surface nucleation sites (density) of a glass substrate is more preferable, because simultaneous planar nucleation will lead to a complete coverage of a silica substrate with TiO_2 nuclei, which will then promote the vertical growth of TiO_2 thin films.

Further Confirmations. To confirm the sequential nucleation observed in previous subsections, the growth of TiO_2 crystallites on scratched glass slides has also been conducted. As shown in Figure 7b−c for an experiment with 0.0100 M TiF_4 at 55 °C for 4 h, more TiO_2 crystallites are distributed along the scratched lines, compared to those on the unscratched areas. More unsaturated chemical bonds such as terminal $Si-O^-$ and anionic vacancies are expected because of the mechanical chipping. Indeed, unlike those in Figure 3a−c, the crystallites are randomly oriented, indicating a simultaneous crystallite growth along the high nucleation density lines. Therefore, the sequentially oriented growth mechanism proposed in Figures 7 and 8 is once again confirmed.

In principle, the mechanical damage does not always produce atomistic nucleation sites across an entire surface, because the chipping occurs preferentially at the places with weak chemical interconnectivity. To create nucleation sites (defects) at the atomic level, a chemical method has been developed in this work. As-received glass slides were treated together with thiourea under hydrothermal conditions, after which a layer of elemental sulfur (tiny hexagonal platelets) was formed. The effect of chemical etching was indicated when the sulfur layer was removed in an ultrasonic bath. As evident in Figure 8a, the glass slide has strongly reacted with thiourea. The surface morphology of the same slide after immersion in 0.0100 M TiF_4 at 60 °C for 3 h is shown in Figure 8b for comparison. Interestingly, a compact TiO_2 film composed of nanocrystallites (mean size = 80 nm) is obtained because high-density nucleation

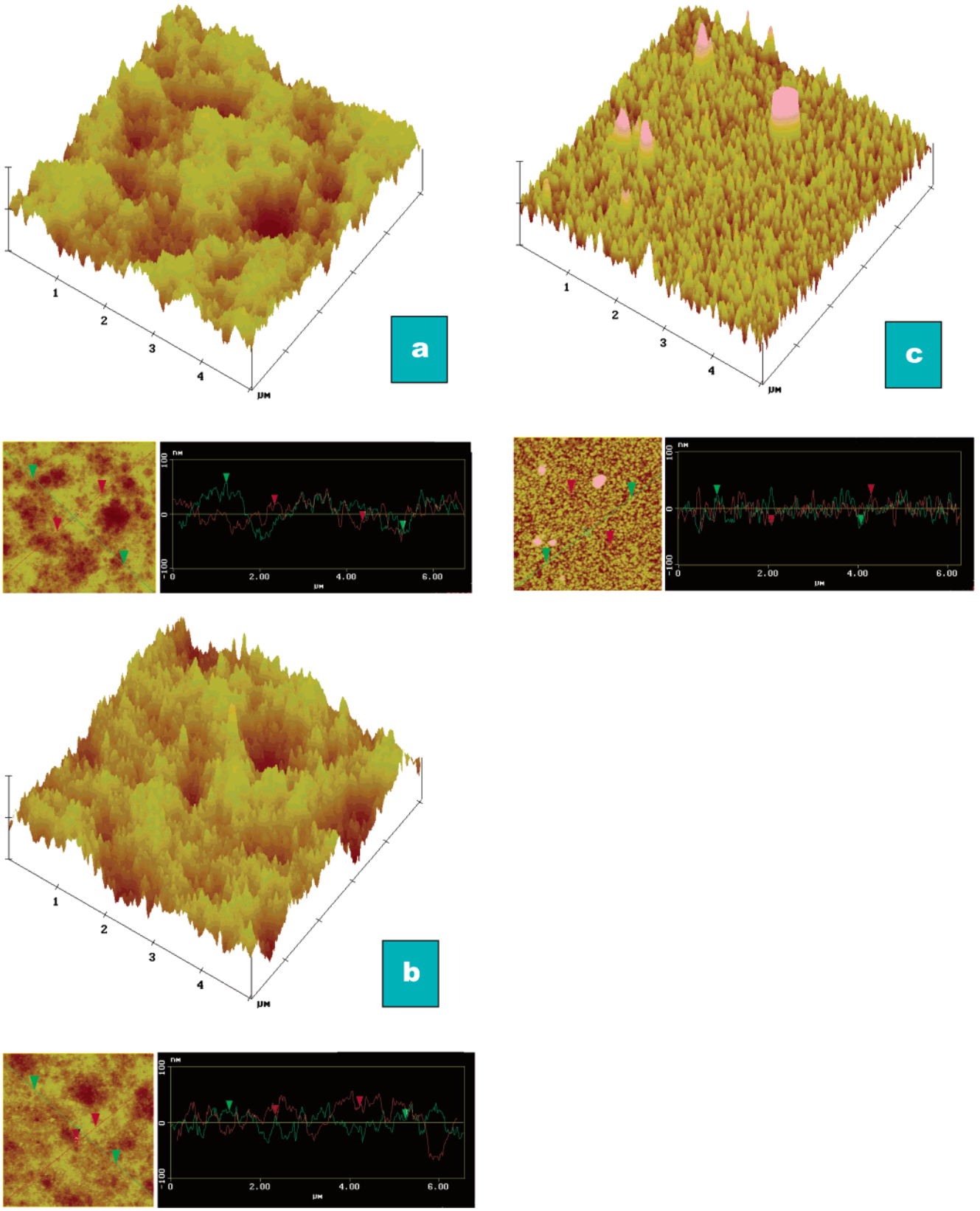

Figure 9. AFM images of the glass modified by thiourea under 200 °C for 74 h (a; standard deviation RMS = 23.0 nm), sample a after 1 h reaction in 0.0100 M TiF_4 at 60 °C (b; pH = 2.0; RMS = 17.4 nm), and sample a after 2 h reaction in 0.0100 M TiF_4 at 60 °C (c; pH = 2.0; RMS = 13.3 nm).

sites have been generated with the chemical pretreatment of the glass substrate. In contrast, under the exactly the same reaction conditions, much larger crystallites (mean size greater than 300 nm) and low nucleation density are observed on unmodified glass because of low nucleation density (lack of atomistic defects, Figure 8c). The nucleation/growth rate of TiO_2 crystallites is much higher on the modified surface. As the skyline structure on the glass substrate is created (Figures 6d, 8a, and 9a), surface affinity between the grown TiO_2 crystallites and the glass surface increases. Furthermore, with this surface

pretreatment, the grown film is composed of nanocrystalline TiO_2 and is fully transparent because its crystallite dimensions are much smaller than the wavelength of visible light.

Figure 9 shows the results of our AFM topographic investigations for the nanocrytalline TiO_2 grown on the modified glass slides. There are numerous etched pits in Figure 9a, which can be classified into (i) relatively large volcano-like "basins" that have been observed with SEM (Figure 8a) and (ii) nanoscale pits within the "basins". After the reaction in 0.0100 M TiF_4 at 55 °C for 2 h, these "basins" are completely full of TiO_2 nanocrystallites (Figure 9c). AFM sectional analysis shows that the nanocrystallites are uniform in size, giving rise to a much flatter TiO_2 thin film.

Results of XPS analysis (Supporting Information) indicate that there is no S element (S 2p)[47] on the chemically etched silica substrate and that the ultrasonic treatment is indeed efficient. More importantly, after only 2 h of growth, Si 2p signals cannot be observed,[49] which indicates that the TiO_2 film has covered the entire etched surface. In agreement with this, O 1s at 532.0 eV of the SiO_2 component disappears completely, while both Ti 2p and O 1s (at 528.8 eV) of TiO_2 reach their maximums.[2−4,30,39] All of these results elucidate that physically or chemically modified substrates can change the growth behavior of TiO_2 and related properties such as porosity, thickness, adhesion, roughness, and transparency of the films.

Conclusions

In summary, we have examined the LPD fundamentals of anatase TiO_2 on fused silica at 55−80 °C with SEM, AFM, TEM, ED, XRD, and XPS methods. Single-crystalline TiO_2 was formed on fused silica during its initial heterogeneous nucleation. The TiO_2 crystal nuclei are elongated along the [001] direction with their [110] axis perpendicular to the glass substrate. Because of an increase in homogeneous nucleation rate, elongated crystallites grew and merged together and later transformed into round flowerlike polycrystalline islands. These islands, formed as individual crystallites and aligned chains, coalesce and form a crystallite monolayer (i.e., TiO_2 thin film). Other growth experiments at different pHs and temperatures have also been investigated. Under the low-pH condition, both heterogeneous nucleation and growth are retarded, but some thin threadlike crystallites would still be seen as self-aligned crystallites. At higher pHs, however, heterogeneous nucleation and its subsequent planar growth are drastically promoted, which gives a poorer homogeneity of crystallites. Chemically, the nucleation and growth of TiO_2 crystallites on fused silica can be described adequately by the hydrolysis of TiF_4 and formation of Si−O−Ti and Ti−O−Ti linkages via condensation and nucleaphilic attachment. One important growth parameter identified in this work is the localized enrichment of HF concentration resulting from TiF_4 hydrolysis, which explains the formation of sequential line assemblies and planar branching, as well as the creation of unsaturated surface bonds (defect sites) of fused glass for heterogeneous nucleation. Our high nucleation density growths using mechanically and chemically treated silica substrates have further confirmed the above findings. Nanocrystalline TiO_2 thin films can be prepared using chemically etched silica substrates.

Supporting Information Available: XRD pattern of detached anatase TiO_2 crystallites and XPS spectra for TiO_2 deposited on unmodified and thiourea-modified glass slides. This material is available free of charge via the Internet at http://pubs.acs.org.

References and Notes

(1) Ishikawa, T.; Yamaoka, H.; Harada, Y.; Fujii, T.; Nagasawa, T. *Nature* **2002**, *416*, 64.

(2) (a) Kim, B.; Byun, D.; Lee, J. K.; Park, D. *Jpn. J. Appl. Phys.* **2002**, *41*, 222. (b) Jung, C. K.; Kang, B. C.; Chae, H. Y.; Kim, Y. S.; Seo, M. K.; Kim, S. K.; Lee, S. B.; Boo, J. H.; Moon, Y. J.; Lee, J. Y. *J. Cryst. Growth* **2002**, *235*, 450. (c) Herman, G. S.; Gao, Y. *Thin Solid Films* **2001**, *397*, 157.

(3) Cacciafesta, P.; Hallam, K. R.; Oyedepo, C. A.; Humphris, A. D. L.; Miles, M. J.; Jandt, K. D. *Chem. Mater.* **2002**, *14*, 777.

(4) Rouse, J. H.; Ferguson, G. S. *Adv. Mater.* **2002**, *14*, 151.

(5) Paranjape, D. V.; Sastry, M.; Ganguly, P. *Appl. Phys. Lett.* **1993**, *63*, 18.

(6) Wang, R.; Hashimoto, K.; Fujishima, A.; Chikuni, M.; Kojima, E.; Kitamura, A.; Shimohigoshi, M.; Watanabe, T. *Nature* **1997**, *388*, 431.

(7) Kato, K.; Tsuzuki, A.; Torii, Y.; Taoda, H.; Kato, T.; Butsugan, Y. *J. Mater. Sci.* **1995**, *30*, 837.

(8) Jiang, F. Z.; Zhang, D. S.; Lin, Y.; Song, Y. L.; Xiao, X. R.; Jiang, L.; Zhu, D. B. *Surf. Interface Anal.* **2001**, *32*, 125.

(9) Yu, J. C.; Yu, J.; Tang, H. Y.; Zhang, L. *J. Mater. Chem.* **2002**, *12*, 81.

(10) Kotov, N. A.; Meldrum, F. C.; Fendler, J. H. *J. Phys. Chem.* **1994**, *98*, 8827.

(11) Lakshmi, B. B.; Dorhout, P. K.; Martin, C. R. *Chem. Mater.* **1997**, *9*, 857.

(12) Lakshmi, B. B.; Patrissi, C. J.; Martin, C. R. *Chem. Mater.* **1997**, *9*, 2544.

(13) Zhang, M.; Bando, Y.; Wada, K. *J. Mater. Sci. Lett.* **2001**, *20*, 167.

(14) Chu, S. Z.; Wada, K.; Inoue, S.; Todoroki, S. I. *Chem. Mater.* **2002**, *14*, 266.

(15) Hoyer, P. *Adv. Mater.* **1996**, *8*, 857.

(16) Hoyer, P. *Langmuir* **1996**, *12*, 1411.

(17) Kobayashi, S.; Hanabusa, K.; Hamasaki, N.; Kimura, M.; Shirai, H.; Shinkai, S. *Chem. Mater.* **2000**, *12*, 1523.

(18) Jung, J. H.; Kobayashi, H.; van Bommel, K. J. C.; Shinkai, S.; Shimizu, T. *Chem. Mater.* **2002**, *14*, 1445.

(19) Kobayashi, S.; Hamasaki, N.; Suzuki, M.; Kimura, M.; Shirai, H.; Hanabusa, K. *J. Am. Chem. Soc.* **2002**, *124*, 6550.

(20) Penn, R. L.; Banfield, J. F. *Science* **1998**, *281*, 969.

(21) Yin, H.; Wada, Y.; Kitamura, T.; Kambe, S.; Murasawa, S.; Mori, H.; Sakata, T.; Yanagida, S. *J. Mater. Chem.* **2001**, *11*, 1694.

(22) Deki, S.; Aoi, Y.; Hiroi, O.; Kajinami, A. *Chem. Lett.* **1996**, 433.

(23) Baskaran, S.; Song, L.; Liu, J.; Chen, Y. L.; Graff, G. L. *J. Am. Ceram. Soc.* **1998**, *81*, 401.

(24) Imai, H.; Takei, Y.; Shimizu, K.; Matsuda, M.; Hirashima, H. *J. Mater. Chem.* **1999**, *9*, 2971.

(25) Imai, H.; Matsuda, M.; Shimizu, K.; Hirashima, H.; Negishi, N. *J. Mater. Chem.* **2000**, *10*, 2005.

(26) Shimizu, K.; Imai, H.; Hirashima, H.; Tsukuma, K. *Thin Solid Films* **2000**, *351*, 220.

(27) Niesen, T. P.; Bill, J.; Aldinger, F. *Chem. Mater.* **2001**, *13*, 1552.

(28) Yamabi, S.; Imai, H. *Chem. Mater.* **2002**, *14*, 609.

(29) Kim, K. J.; Benkstein, K. D.; van der Lagemaat, J.; Frank, A. J. *Chem. Mater.* **2002**, *14*, 1042.

(30) Masuda, Y.; Jinbo, Y.; Yonezawa, T.; Koumoto, K. *Chem. Mater.* **2002**, *14*, 1236.

(31) (a) Meyer zu Heringdorf, F. J.; Reuter, M. C.; Tromp, R. M. *Nature* **2001**, *412*, 517. (b) Chamber, S. A.; Droubay, T.; Jennison, D. R.; Mattsson, T. R. *Science* **2002**, *297*, 827.

(32) (a) Yoldas, B. E.; O'Keeffe, T. W. *Appl. Opt.* **1979**, *18*, 3133. (b) Butler, M. A.; Ginley, D. S. *J. Mater. Sci.* **1980**, *15*, 19.

(33) Carlson, T.; Giffin, G. L. *J. Phys. Chem.* **1986**, *90*, 5896.

(34) Burns, G. P. *J. Appl. Phys.* **1989**, *65*, 2095.

(35) Matsunaga, T.; Tomoda, R.; Nakajima, T.; Komine, T. *Appl. Environ. Microbiol.* **1988**, *54*, 330.

(36) (a) Wang, C. M.; Mallouk, T. E. *J. Phys. Chem.* **1990**, *94*, 4276. (b) Wang, C. M.; Mallouk, T. E. *J. Am. Chem. Soc.* **1990**, *112*, 2016.

(37) Borenstain, S. I.; Arad, U.; Lyubina, I.; Segal, A.; Warschawer, Y. *Thin Solid Films* **1999**, *75*, 2659.

(38) Peercy, P. S. *Nature* **2000**, *406*, 1023.

(39) Meng, Q. B.; Fu, C. H.; Einaga, Y.; Gu, Z. Z.; Fujishima, A.; Sato, O. *Chem. Mater.* **2002**, *14*, 83.

(40) Bullen, H. A.; Garrett, S. J. *Nano Lett.* **2002**, *2*, 739.

(41) Gu, Z. Z.; Fujishima, A.; Sato, O. *Chem. Mater.* **2002**, *14*, 760.

(42) (a) Nazeeruddin, M. K.; Kay, A.; Rodicio, I.; Humphry-Baker, R.; Muller, E.; Liska, P.; Vlachopoulos, N.; Gratzel, M. *J. Am. Chem. Soc.* **1993**, *115*, 6382. (b) Bach, U.; Lupo, D.; Comte, P.; Moser, J. E.; Weissortel, F.; Salbeck, J.; Spreitzer, H.; Gratzel, M. *Nature* **1998**, *395*, 583. (c) Gratzel, M. *Nature* **2001**, *414*, 338.

(43) Wijnhoven, J. E. G.; Vos, W. L. *Science* **1998**, *281*, 802.

(44) Schmitt, R. H.; Glove, E. L.; Brown, R. D. *J. Am. Chem. Soc*. **1960**, *82*, 5292.
(45) Xu, Z. P.; Zeng, H. C. *J. Phys. Chem. B* **2001**, *105*, 1743.
(46) Zeng, H. C.; Ng, W. K.; Cheong, L. H.; Xie, F.; Xu, R. *J. Phys. Chem. B* **2001**, *105*, 7178.
(47) Zeng, H. C.; Xie, F.; Wong, K. C.; Mitchell, K. A. R. *Chem. Mater*. **2002**, *14*, 1788.
(48) Sampanthar, J. T.; Zeng, H. C. *J. Am. Chem. Soc*. **2002**, *124*, 6668.
(49) Teo, S. H.; Zeng, H. C. *J. Phys. Chem. B* **2001**, *105*, 9093.
(50) Chemseddine, A.; Moritz, T. *Eur. J. Inorg. Chem*. **1999**, 235.
(51) (a) Aruna, S. T.; Tirosh, S.; Zaban, A. *J. Mater. Chem*. **2000**, *10*, 2388. (b) Kasuga, T.; Hiramatsu, M.; Hoson, A.; Sekino, T.; Niihara, K. *Langmuir* **1998**, *14*, 3160.
(52) (a) Liang, Y.; Gan, S.; Chambers, S. A.; Altman, E. I. *Phys. Rev. B* **2001**, *63*, 235402. (b) Hengerer, R.; Bolliger, B.; Erbudak, M.; Gratzel, M. *Surf. Sci*. **2000**, *460*, 162.
(53) Comba, P.; Merbach, A. *Inorg. Chem*. **1987**, *26*, 1315.
(54) Hildenbrand, V. D.; Fuess, H.; Pfaff, G.; Reynders, P. *Z. Phys. Chem*. **1996**, *194*, 139.
(55) Zheng, Y.; Shi, E.; Chen, Z.; Li, W.; Hu, X. *J. Mater. Chem*. **2001**, *11*, 1547.
(56) Yin, H.; Wada, Y.; Kitamura, T.; Kambe, S.; Murasawa, S.; Mori, H.; Sakata, T.; Yanagida, S. *J. Mater. Chem*. **2001**, *11*, 1694.
(57) Zeng, H. C.; Tanaka, K.; Hirao, K.; Soga, N. *J. Non-Cryst. Solids* **1997**, *209*, 112.
(58) Iler, R. K. *The Chemistry of Silica*; Wiley-Interscience: New York, 1979; pp 387−390.
(59) Lin, Z.; Rocha, J.; Pedrosa de Jesus, J. D.; Ferreira, A. *J. Mater. Chem*. **2000**, *10*, 1353.
(60) Ferreira, P.; Ferreira, A.; Rocha, J.; Soares, M. R. *Chem. Mater*. **2001**, *13*, 355.
(61) Wang, C.; Zhang, Y.; Dong, L.; Fu, L.; Bai, Y.; Li, T.; Xu, J.; Wei, Y. *Chem. Mater*. **2000**, *12*, 3662.